



This is a repository copy of *Rotor Position Estimation of a Pseudo Direct Drive PM machine using Extended Kalman Filter*.

White Rose Research Online URL for this paper:  
<http://eprints.whiterose.ac.uk/109769/>

Version: Accepted Version

---

**Article:**

Bouheraoua, M., Wang, J. [orcid.org/0000-0003-4870-3744](https://orcid.org/0000-0003-4870-3744) and Atallah, K. (2017) Rotor Position Estimation of a Pseudo Direct Drive PM machine using Extended Kalman Filter. *IEEE Transactions on Industry Applications*, 53 (2). pp. 1088-1095. ISSN 0093-9994

<https://doi.org/10.1109/TIA.2016.2619326>

---

© 2016 IEEE. Personal use of this material is permitted. Permission from IEEE must be obtained for all other users, including reprinting/ republishing this material for advertising or promotional purposes, creating new collective works for resale or redistribution to servers or lists, or reuse of any copyrighted components of this work in other works.

**Reuse**

Unless indicated otherwise, fulltext items are protected by copyright with all rights reserved. The copyright exception in section 29 of the Copyright, Designs and Patents Act 1988 allows the making of a single copy solely for the purpose of non-commercial research or private study within the limits of fair dealing. The publisher or other rights-holder may allow further reproduction and re-use of this version - refer to the White Rose Research Online record for this item. Where records identify the publisher as the copyright holder, users can verify any specific terms of use on the publisher's website.

**Takedown**

If you consider content in White Rose Research Online to be in breach of UK law, please notify us by emailing [eprints@whiterose.ac.uk](mailto:eprints@whiterose.ac.uk) including the URL of the record and the reason for the withdrawal request.



[eprints@whiterose.ac.uk](mailto:eprints@whiterose.ac.uk)  
<https://eprints.whiterose.ac.uk/>

# Rotor Position Estimation of a Pseudo Direct Drive PM machine using Extended Kalman Filter

Mohammed Bouheraoua

Control Systems  
Magnomatics Limited  
Sheffield, UK

m.bouheraoua@magnomatics.com

Jiabin Wang and Kais Atallah

Electronic and Electrical Engineering  
The University of Sheffield  
Sheffield, UK

**Abstract** - The paper describes an improved method to control a Pseudo Direct Drive (PDD) permanent magnet machine with only one sensor on the low-speed rotor (LSR). Due to the magnetic coupling between the two rotors, the PDD machine exhibits low stiffness and non-linear torque transmission characteristics, and hence, the position of the high-speed rotor (HSR) cannot be determined using a simple gear ratio relationship. An extended kalman filter is proposed to accurately estimate the position of the HSR which is used to provide electronic commutation for the drive. The technique has been implemented on a prototype PDD subjected to various speed and load torque profiles.

**Index Terms**-- Electric Drives, Magnetic Gear, Permanent Magnet Machine, Pseudo Direct Drive, PDD, Extended Kalman Filter, Slip, State Feedback Control, Wind Turbine.

## I. INTRODUCTION

A PDD permanent magnet (PM) machine, is realised by the mechanical and magnetic integration of a PM machine and a magnetic gear, and can achieve torque densities larger than  $60\text{kNm/m}^3$  [1], for medium to small size, with an airgap shear stress in excess of  $75\text{kN/m}^2$ . However, for larger PDDs airgap shear stress values of the order of  $110\text{kN/m}^2$  can be reached [2], with low cogging torque, and a high power factor ( $> 0.9$ ), these shear stress values are significantly larger than the typical values of  $40\text{--}50\text{kPa}$ , encountered in wind turbine direct drive PM generators, [3]. The PDD alleviates the problems associated with a mechanical gearbox, such as acoustic noise and vibrations, the need for lubrication and maintenance, and minimises the risk of failures associated with fatigue and jamming, such application include, ship propulsion, wind turbine generators, land transportation and aerospace actuation. Albeit at slightly increased capital cost, but with potentially reduced lifetime costs. Figures 1 shows 3D and cross-sectional schematics of a PDD machine, where the electromagnetic torque is produced by the interaction of the 2 pole-pair magnets ( $p_h = 2$ ) on the HSR with the currents

in the stator winding. This torque is transmitted to the LSR, with a gear ratio  $G_r = n_s/p_h$ , by the interaction of the 21 pole-pair ( $p_l = 21$ ) stationary permanent magnets attached to the stator bore and the 21<sup>st</sup> asynchronous space harmonic resulting from the modulation of the 2 pole-pair magnetic field on the HSR by the 23 ( $n_s = 23$ ) ferromagnetic pole-pieces of the LSR where the load is connected. In addition to the problems associated with practical controllers, e.g. signal noise and delays, in a PDD the torque is transmitted to the load through a relatively low stiffness magnetic gear, thus, undesirable speed/position oscillations may be present if conventional controllers, such as PID, are employed. Furthermore, overload protection is a significant advantage of a PDD, since when subjected to a load torque which is greater than the pull-out torque, the two rotors would harmlessly slip. Although this may not result in a physical damage, the time taken for the machine to recover and resume normal operation after the transient overload torque disappears, will depend on how quickly the slip can be detected and how the control strategy adapts to these changes.

The servo control which includes two inertias connected by a compliant mechanical coupling has been studied in [4],[5] and [6]. It is shown that the inertia ratio between the load and motor directly affects the performance of the controller in terms of suppressing resonance oscillation. A torque transducer is utilised together with Integral Proportional (IP) control in [5] and [7] to reduce the undesirable oscillation. However, the use of a torque transducer not only increases drive system cost but also compromises mechanical simplicity.

A load torque disturbance observer is proposed in [8] as a means of feedback to improve the system damping. This scheme is, however, sensitive to measurement noise, parameter variations and non-linearity in the observer model. More recently, a comprehensive analysis and design techniques for speed control of compliant and rigid systems

---

The work is carried out with the support of the UK EPSRC, and Magnomatics Ltd through the provision of a PhD studentship.

have been reported in [9],[10] and using IP or PI based control. These controllers have been optimally tuned and compared with state feedback controller, with the latter exhibiting superior performance in reducing the oscillations associated with the low and non-linear stiffness of the magnetic gear [11].

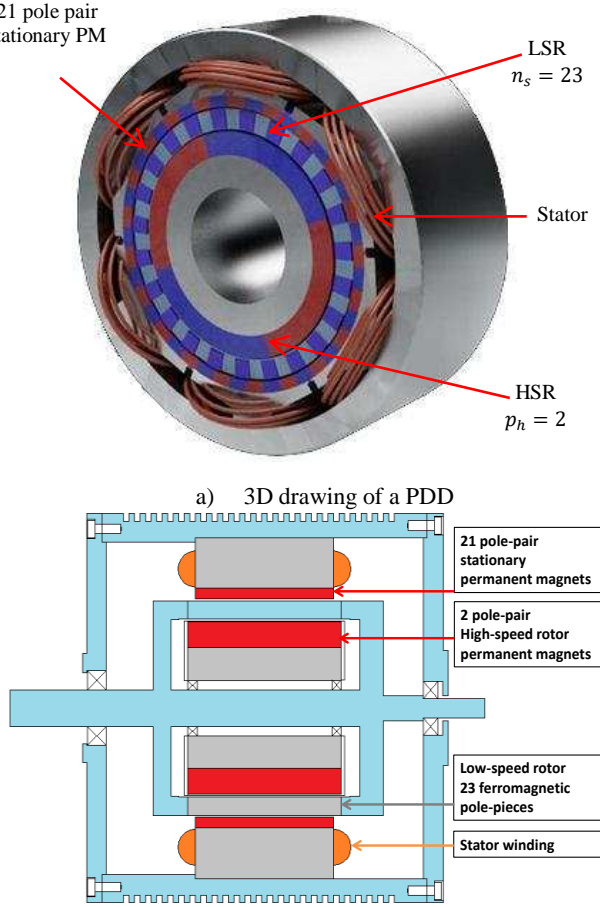


Fig. 1. PDD structure

A drive train composed of a motor and load connected through a compliant 1:1 magnetic coupling, where the inertia ratio between the motor and the load is close to unity has been demonstrated in [12],[13]. Since the magnetic coupling is far more flexible than a conventional mechanical coupling with medium torsional stiffness, oscillations appear on the load side if conventional control is used. It has been shown that the IP control optimally tuned against the fourth-order integral time multiplied by absolute error (ITAE) polynomial can have good oscillation rejection characteristics. However, the magnetic coupling presented in [13] exhibits damping torque caused by the eddy currents generated in its solid back-irons. This damping together with the well-tuned IP control is adequate in reducing the

undesirable oscillation. In contrast, the PDD exhibits very little damping, because in order to maximise efficiency, it is manufactured using laminated electrical steel. Consequently, eddy current losses are minimised. In addition to the low stiffness coupling, the gearing in a PDD machine has significant effect on the inertia ratio between the HSR and the LSR. Hence, the controller structure and design presented for the magnetic coupling may not provide sufficient damping for the PDD operation.

Previous work on the PDD control has implemented a reduced order observer with a single sensor mounted on the LSR to provide a feedback signal for the speed controller and electronic commutation for the drive to perform PWM switching, in large PDDs the HSR must be fully encapsulated inside the LSR to improve mechanical integrity, hence the HSR speed/position cannot be measured [14]. A linear reduced observer has been implemented to estimate the speed and position of the HSR based on a measured LSR position. However, due to non-linear torque transmission relationship between the HSR and the LSR the linear observer designed at a fixed operating point around the rated torque incurs position estimation error. Thus, when operating under other load conditions the PDD performance is not optimised. For the PDD to operate with optimal performance while torque and speed operating points change continuously, the position of the HSR should be estimated using a non-linear observer to improve estimation accuracy.

The paper proposes a novel implementation of an Extended Kalman Filter (EKF) on a PDD. It is experimentally and theoretically shown that the adaptive nonlinear observer can provide accurate position estimation for the HSR and ensures optimum PDD operation under variable load conditions. The EKF is tuned by genetic algorithm (GA) against a defined set of criteria and its performance is compared with the linear observer and tested on prototype PDD machine.

## II. MODELLING OF THE PSEUDO DIRECT DRIVE

The electrical dynamics of the PDD is similar to that of the conventional surface mounted brushless permanent magnet machine. They are given in term of the d-q axis currents  $i_d$  and  $i_q$ , by

$$\frac{di_d}{dt} = -\frac{R}{L_d}i_d + \frac{\omega_s L_q i_q}{L_d} + \frac{v_d}{L_d} \quad (1)$$

$$\frac{di_q}{dt} = -\frac{R}{L_q}i_q - \frac{\omega_s L_d i_d}{L_q} + \frac{v_q - K_e \omega_h}{L_q} \quad (2)$$

$L_d$  and  $L_q$  are the d- and q-axis motor inductances, respectively;  $R$  is the motor winding resistance per phase;  $K_e = p_h \phi_m$  is the motor back-emf constant.  $v_d$  and  $v_q$  are d- and q-axis voltages, respectively.  $\omega_h$  is the speed of the HSR, and  $\omega_s = p_h \omega_h$  is the electrical angular frequency of the HSR.

In a PDD, the HSR and the LSR are magnetically coupled and the mechanical load is applied to the LSR. The torque is transmitted from HSR to the LSR. The equations that govern their motion are as follows:

$$\frac{d\omega_h}{dt} = \frac{T_e}{J_h} - \frac{T_{max}}{J_h G_r} \sin(\theta_e) - \frac{B_h}{J_h} \omega_h - \frac{K_d}{J_h} (p_h \omega_h - n_s \omega_o) \quad (3)$$

$$\frac{d\omega_o}{dt} = \frac{T_{max}}{J} \sin(\theta_e) - \frac{B_o}{J} \omega_o + \frac{K_d G_r}{J} (p_h \omega_h - n_s \omega_o) - \frac{T_L}{J} \quad (4)$$

where,  $J_h, B_h$  are the moment of inertia and the viscous damping of the HSR, respectively.  $\omega_o, J, B_o$  are the angular speed, the combined inertia of the LSR  $J_o$  and the load  $J_L$ , and the combined damping coefficient of the low-speed rotor and the load, respectively. The damping coefficient  $K_d$  is associated with the referred angular speed  $\frac{d\theta_e}{dt}$  between the HSR and the LSR. In this PDD damping is very small, therefore it is neglected in the analysis and  $B_h = B_o = K_d = 0$ . The resulting signal flow graph of the PDD is shown in Fig. 2.  $G_r = n_s/p_h$  is the magnetic gear ratio, where  $p_h$  is the number of pole-pairs on the HSR and  $n_s$  is the number of ferromagnetic pole piece on the LSR.  $T_L$  is the load torque,  $T_{max}$  is the pull-out torque reflected to the LSR and  $T_e$  is the electromagnetic torque produced by the q- axis current  $i_q$ , when a surface-mounted magnet topology is employed for the HSR, and is given by :

$$T_e = K_t i_q, \quad K_t = \frac{3}{2} p_h \phi_m \quad (5)$$

$K_t$  is the motor torque constant,  $\phi_m$  is the stator flux-linkage due to permanent magnets.

$$\theta_e = p_h \theta_h - n_s \theta_o = \int (p_h \omega_h - n_s \omega_o) dt \quad (6)$$

$\theta_e$  is defined as the referred angular displacement between the HSR and the LSR.

$\theta_h$  and  $\theta_o$  are the angular positions of the HSR and LSR, respectively. The stiffness of the magnetic gear is positive only when  $\theta_e$  is within the range

$2\pi n - \frac{\pi}{2} < \theta_e < 2\pi n + \frac{\pi}{2}$ ,  $n$  is an integer number. The equivalent stiffness decreases as  $\theta_e$  approaches  $\frac{\pi}{2}$ .

The equivalent inertia of the HSR with the magnetic gear seen by the LSR is obtained by:

$$J_e = G_r^2 J_h \quad (7)$$

It has been shown that due to lack of damping in the magnetic gear with relatively low stiffness, resonant

oscillation may occur in speed or position responses of the low-speed rotor [15].

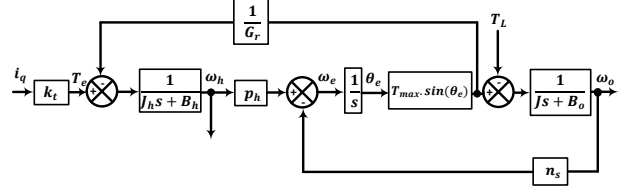


Fig. 2. Transfer function block diagram

The PDD parameters are given in table 1

Parameter	Value
$J_h (kgm^2)$	$3.8 \times 10^{-3}$
$J_o (kgm^2)$	$2.5 \times 10^{-3}$
$J_L (kgm^2)$	0.28
$R (\Omega)$	2
$\phi_m (Wb)$	0.59
$T_{max} (Nm)$	120
$L_d (H)$	$32.6 \times 10^{-3}$
$L_q (H)$	$32.6 \times 10^{-3}$
$\omega_{o,max} (rad/s)$	30
$\omega_{h,max} (rad/s)$	345
$U_{dc} (V)$	435
$i_{q,max} (A)$	9
$K_{\omega_h} (A/rad/s)$	2
$K_{\omega_o} (A/rad/s)$	1.69
$K_{\theta_e} (A/rad/s)$	9.78
$K_s (dimensionless)$	0.5
$K_i (1/s)$	210

### III. CONTROL STRATEGY AND EKF DESIGN

The presence of the oscillatory mode in the PDD machine transfer function has introduced some challenging control issues. When a conventional PI control had been implemented in the speed controller, undesirable oscillations appear on the output (LSR). This problem has been addressed by the state feedback (SFBK) controller structure shown in Fig. 3.

$$u = [(\omega_d - \omega_h) + (\omega_o \cdot G_r - \omega_h) \cdot K_s] \frac{K_i}{s} - \omega_h \cdot K_{\omega_h} - \omega_o \cdot K_{\omega_o} - \theta_e \cdot K_{\theta_e} \quad (8)$$

The state feedback controller generates current reference which is tracked by the inner current control loop employing the field oriented control strategy. The proportional gains,  $K_{pd}$  and  $K_{pq}$ , and the integral gains  $K_{id}$  and  $K_{iq}$ , of the d- and q-axis current controller are designed for a bandwidth of 400Hz using the zero-pole cancellation method [16]. The speed control gains  $K_{\omega_h}$ ,  $K_{\omega_o}$  and  $K_{\theta_e}$  are associated with the feedbacks of the HSR speed  $\omega_h$ , the LSR speed  $\omega_o$  and the referred load angle  $\theta_e$ , respectively.

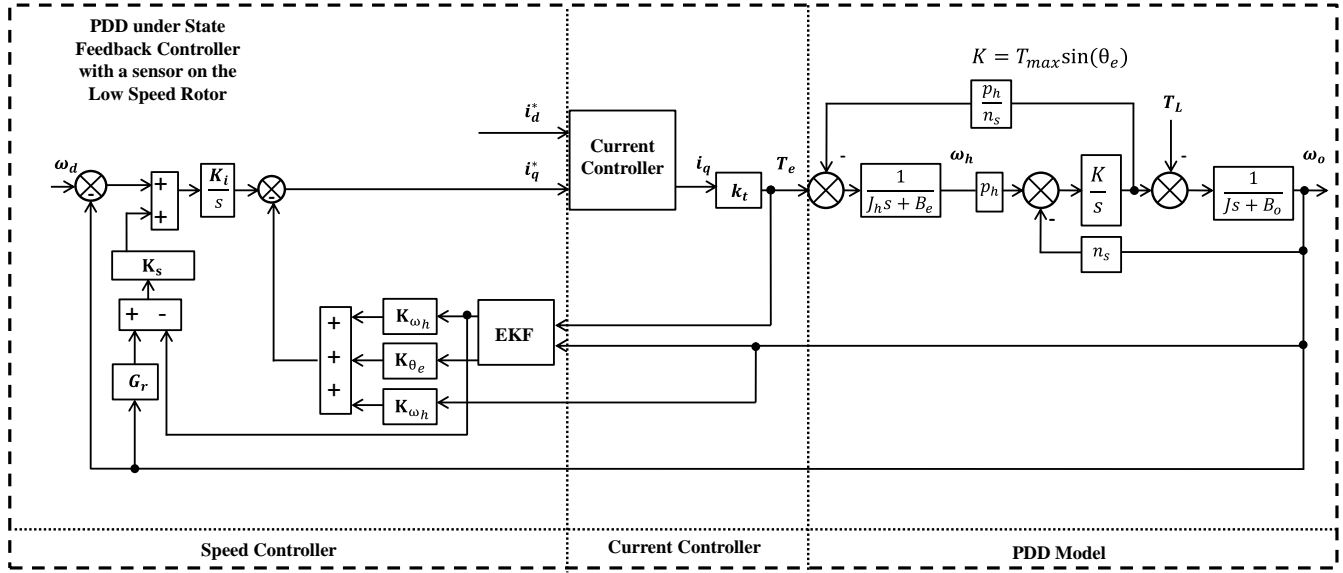


Fig. 3. Schematic of the PDD under the EKF based state feedback controller.

The fourth proportional gain  $K_s$  is specifically introduced to limit any deviation in the gear ratio between the two rotors during transient events, hence reducing the probability of controller induced slip of the magnetic gear element of the PDD. In steady state this gain has no or very little effect on the feedback system as can be seen in (8). The integral gain  $K_i$  is used to eliminate steady state error. The output of the SFBK is expressed as follows:

The gains of the state feedback controller are optimally tuned with genetic algorithm (GA) to satisfy the (ITAE) criteria as well as voltage and current constraints. The details about the definition of the ITAE criteria and tuning method can be found in [17] a time and frequency domain analysis of the PDD is provided in [11].

In order to implement the full state feedback control strategy shown in Fig. 3, the unmeasured feedback signals of  $\omega_h$ ,  $\theta_e$  are necessary for the control strategy. In addition, the angular position of the HSR is required for electronic commutation of the commercial drive. However, direct measurements of these signals ( $\omega_h$ ,  $\theta_e$ ) are not available and hence EKF is used to estimate these unmeasured states. Therefore measured  $\omega_o$  is fed to EKF to update its output  $y$  in (16) and hence EKF updates the estimations of ( $\omega_h$ ,  $\theta_e$ ), the EKF input is  $u$ .

$$\dot{x} = f(x) + Bu + w(t) \quad (9)$$

$$y = Cx + v(t)$$

$$x = [\omega_h, \omega_o, \theta_e, T_L]^T \quad (10)$$

$$B = \left[ \frac{1}{J_h}, 0, 0, 0 \right]^T$$

$$C = [0, 1, 0, 0]$$

$$u = T_e$$

$$f(x) = [f_1(x), f_2(x), f_3(x), f_4(x)]^T$$

$$f_1(x) = -\frac{T_{max}}{J_h G_r} \sin(\theta_e)$$

$$f_2(x) = \frac{T_{max}}{J} \sin(\theta_e) - \frac{T_L}{J} \quad (11)$$

$$f_3(x) = p_h \omega_h - n_s \omega_o$$

$$f_4(x) = 0$$

The Jacobian matrix  $F(x) = \frac{\partial f(x, u)}{\partial x}$  is given by:

$$F(x) = \begin{bmatrix} 0 & 0 & -\frac{T_{max}}{J_h G_r} \cos(\theta_e) & 0 \\ 0 & 0 & \frac{T_{max}}{J} \cos(\theta_e) & -\frac{1}{J} \\ p_h & -n_s & 0 & 0 \\ 0 & 0 & 0 & 0 \end{bmatrix} \quad (12)$$

The EKF description, equation (9), is based on the PDD mechanical governing equations (10) and (11) and the assumption that the time derivative of the load torque is zero. The input  $u$  and  $B$ ,  $C$  matrices are given in (10), and the vector function  $f(x)$  and its Jacobian matrix are given in

(12). They are used to design an EKF observer based on the input  $u$  and output  $y$  [18]. According to the Kalman filter theory the system is disturbed by Gaussian process and measurement noises,  $w(t)$  and  $v(t)$ , and their covariance matrices are denoted by  $Q$  and  $R_d$ , respectively.

After discretisation at the  $k^{th}$  sample instant, the optimal state estimate,  $x_{k|k}$  and the estimation error covariant matrix  $P_{k|k}$  are obtained through a simplified EKF algorithm over two steps:

**Prediction step** where a simple forward Euler technique is used so that the prediction step results in the following recursive equations:

$$x_{k|k-1} = x_{k-1|k-1} + [f(x_{k-1|k-1}) + Bu_{k-1}]T_c \quad (13)$$

$$P_{k|k-1} = P_{k-1|k-1} + [F_{k-1}P_{k-1|k-1} + P_{k-1|k-1}F_{k-1}^T]T_c + Q \quad (14)$$

The **innovation step** corrects the prediction estimation and its error covariance matrix by:

$$K_k = P_{k|k-1}C^T(CP_{k|k-1}C^T + R_d)^{-1} \quad (15)$$

$$x_{k|k} = x_{k|k-1} + K_k[y_k - Cx_{k|k-1}] \quad (16)$$

$$P_{k|k} = P_{k|k-1} - K_kCP_{k|k-1} \quad (17)$$

where,

$T_c$	Sampling interval
$k$	Sampling instant
$Q$	Covariance matrix associated with the process noise
$R_d$	Covariance matrix associated with measurement noise
$x_{k k-1}$	Predicted state estimate
$x_{k k}$	Optimal state estimate
$P_{k k-1}$	Predicted error covariance matrix
$P_{k k}$	Optimal error covariance matrix
$K_k$	Adaptive Kalman filter gain

It is well known that the EKF performance in transient and steady state, is heavily influenced by the choice of the matrices  $Q$  and  $R_d$ . It has also been reported in the literature that the analytical guidelines which ensure proper setting of these matrices do not exist [19] [20] and linearization methods may be used [21] [22] or manual tuning using trial and error is assumed since no systematic tuning method has been reported [23]. However, trial and error is time consuming and does not guarantee optimal EKF performance. Therefore, GA has been chosen to optimise the  $Q$  and  $R_d$  matrices based on the performance index given in (18)

$$P_i = \min \sum_{n=1}^n |\omega_{h_{model}}(n) - \omega_{h_{EKF}}(n)| \quad (18)$$

where  $P_i$  is the performance index,  $n$  is the number of samples,  $\omega_{h_{model}}$  is the HSR speed from the simulated model,  $\omega_{h_{EKF}}$  is the estimated HSR speed from the EKF observer.

The initial diagonal matrix  $P_0$  represents the mean square errors, given the initial condition of the system. Increasing  $P_0$  affects the amplitude of the transient while the duration of the transient and the steady state condition remain unaffected [18] [20]. The  $Q$  matrix gives information about the system noise level and large values of the elements in  $Q$  would indicate the presence of large noise in the system or increase in parameter uncertainties. This will result in an increase of the Kalman gain, and consequently the filter will have a faster dynamics. The  $R_d$  matrix is associated with the measurement noise. Increasing the value of its elements would indicate large noise in the measurements and yields a decrease in the Kalman gain, resulting in a slow transient performance. As a common practice the matrices  $Q$ ,  $R_d$  and  $P_0$  are chosen to be diagonal, since the off-diagonal terms have less effect on the performance of the EKF [18] [20]. Furthermore,  $Q$  and  $R_d$  matrices depend on the sampling time, drive system parameters, measurement amplitude and noise level. Therefore, GA has been employed to tune the elements,  $q_1, q_2, q_3, q_4$  and  $r_1$ , offline using the non-linear model of the PDD in Simulink as shown in fig. 3 with sampling frequency of 10kHz. The goal of tuning is to minimise the performance index (18) [17].

$$Q = \begin{bmatrix} q_1 & 0 & 0 & 0 \\ 0 & q_2 & 0 & 0 \\ 0 & 0 & q_3 & 0 \\ 0 & 0 & 0 & q_4 \end{bmatrix}, \quad R_d = r_1 \quad (19)$$

$$q_1 = 1, \quad q_2 = 0.01, \quad q_3 = 0.001, \quad q_4 = 10, \quad R_d = 26,$$

Since  $P_0$  has little influence on the EKF behavior it has been initialized to be a unity matrix

$$P_0 = \begin{bmatrix} 1 & 0 & 0 & 0 \\ 0 & 1 & 0 & 0 \\ 0 & 0 & 1 & 0 \\ 0 & 0 & 0 & 1 \end{bmatrix} \quad (20)$$

Once the elements of the matrices  $Q$  and  $R_d$  have been tuned offline the new parameters are loaded to dSPACE real-time, where the PDD machine is used instead of the model.

#### IV. EXPERIMENTAL RESULTS AND DISCUSSION

Once the tuning is completed, the EKF is employed to estimate the unmeasured states to be used for the SFBK controller and to reconstruct the HSR angular position for the electronic commutation of the drive. It has been shown in [14] that direct integration of the estimated speed of the HSR results in accumulative error in the estimated HSR position, the error increment can be seen between the measured and estimated positions of the HSR; it is due to the compliant coupling of the magnetic gear in transient. The difference will give rise to torque control error, reduction in efficiency, and deterioration in transient response. To circumvent this problem the position of the HSR is given by:

$$\hat{\theta}_h = \frac{1}{p_h} \hat{\theta}_e + \frac{n_s}{p_h} \theta_o \quad (21)$$

where  $\hat{\theta}_h$  is the estimated position of the HSR,  $\hat{\theta}_e$  is estimated referred angle.

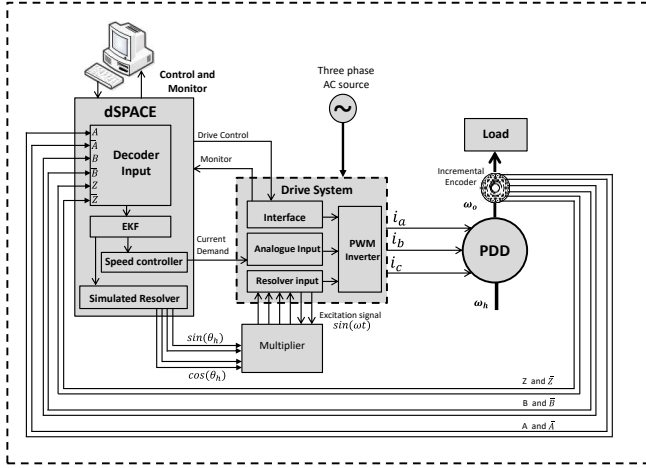


Fig. 4. Schematic of closed-loop speed control of PDD machine using LSR sensor.

Fig. 4 shows the real-time realisation of the feedback system in Fig. 3. The state feedback control strategy and the observer algorithm are implemented on a dSPACE real-time control platform. The speed of the LSR is measured using an incremental encoder with a resolution of 1024 pulses per revolution through the standard dSPACE encoder interface. The estimated position of the HSR is converted into sine and cosine which are fed to the a bespoke multiplier converter to produce a resolver-like signal which is used via a standard resolver interface for control of the d- and q- axis currents using a commercial drive unit. This conversion is not necessary if the state feedback control and the observer are integrated into the drive control. The  $i_q$  current demand resulted from the speed controller is sent to the commercial drive as the reference current demand. The drive performs electronic commutation and current control using the estimated position signal for the HSR and the  $i_q$  demand.



Fig 5. Pseudo Direct Drive test Rig

To evaluate the EKF performance and the accuracy of the position estimation for the HSR, the prototype PDD used in the test has an accessible shaft on the HSR to fit a measurement sensor. A resolver is then attached to the shaft for the purpose of monitoring its speed/position only.

Fig 5 shows the PDD test rig where the PM load machine is coupled to the PDD via a 10:1 inline gear box in order to provide sufficient load torque for the PDD operation. The torque command generated by the dSPACE controller is fed to the commercial drive configured in torque control mode. The PDD operates in speed control mode and is loaded by the PM machine in torque control mode. Using the position feedback from the machines and torque reference from the real-time controller, the drive performs current regulation and electronic commutation via a 3-phase inverter. PWM switching is performed at 8 kHz for both drives to minimize electromagnetic interference.

The PDD can be tested to validate the following

- The ability to maintain reference speed against a large load torque variation.
- The ability to start the PDD fully loaded from stand still
- The ability to maintain same torque per Amp in both forward and reverse motoring.

To assess the PDD performance, a test profile is designed to evaluate the above criteria. The LSR is accelerated to 100rpm from standstill and a step load of 100Nm equivalent to the PDD rated torque is applied at  $t = 2s$  for the duration of 3s. The PDD starts to decelerate to zero rpm at  $t = 6s$ . At  $t = 8s$  the PDD starts in reverse direction to -100rpm with the same load torque for the duration of 4s. At  $t = 12s$  the load is removed. The reference speed of the PDD is set to zero at  $t = 14s$ .

The load torque applied to the PDD in the simulation was 100 Nm, whereas, the load torque applied to the prototype PDD in testing was 112 Nm, and this is due to the machine being cold and friction in the drive train including the mechanical gearbox, this can also be seen on the q-current and the referred angle.

Fig. 6a shows the speed responses of the HSR, both simulated, EKF estimated, Fig 6b shows the measured and EKF estimated speed of the HSR given the measured LSR.

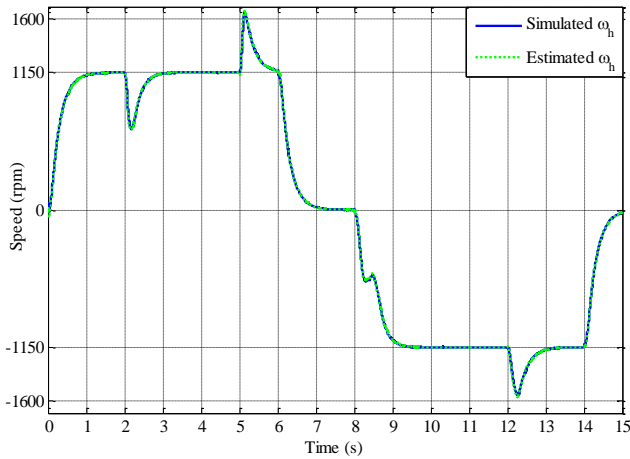


Fig 6a. Simulated and EKF estimated  $\omega_h$

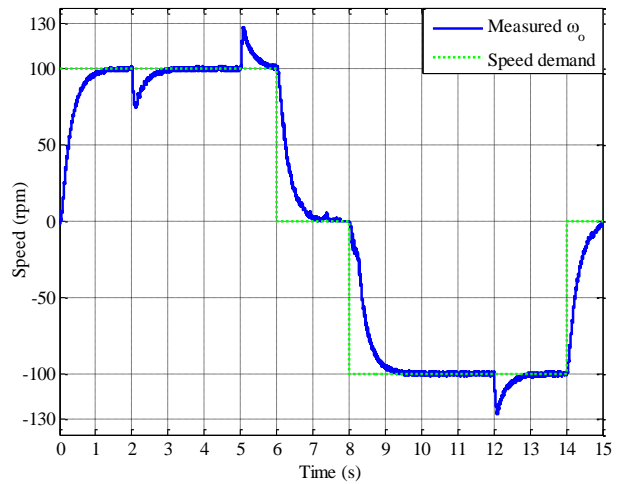


Fig 7b. Measured  $\omega_o$

Figs. 8a and 8b show the dq-axis current resulting from the test profile of the PDD under EKF simulated and measured respectively, it can be seen that  $i_q$  current has the same values in both motoring directions. It can also be seen that PWM generated ripple exists on measured currents.

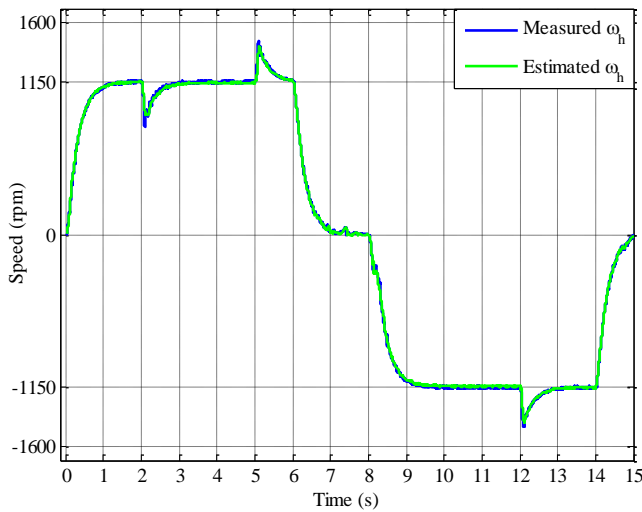


Fig 6b. Measured and EKF estimated  $\omega_h$

Fig. 7a shows the simulated and estimated speed of the LSR, Fig 7b shows the measured LSR, it tracks the reference speed very well in both forward and reverse motoring when subject to the load torque profile.

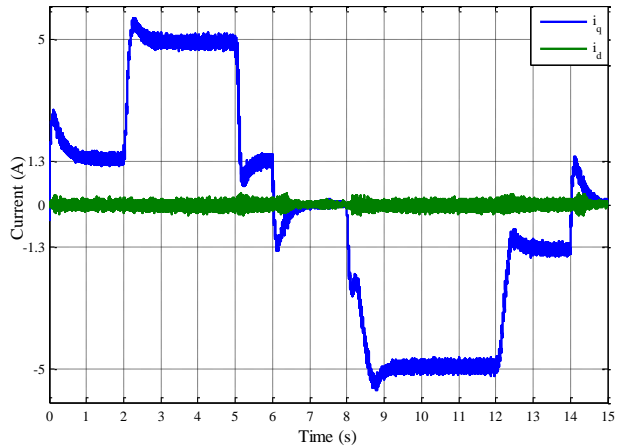


Fig 8a. Simulated  $i_q$  and  $i_d$  currents

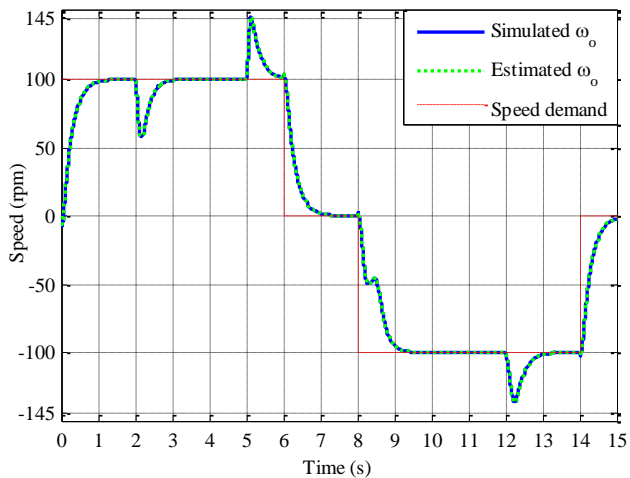


Fig 7a. Simulated and EKF estimated  $\omega_o$

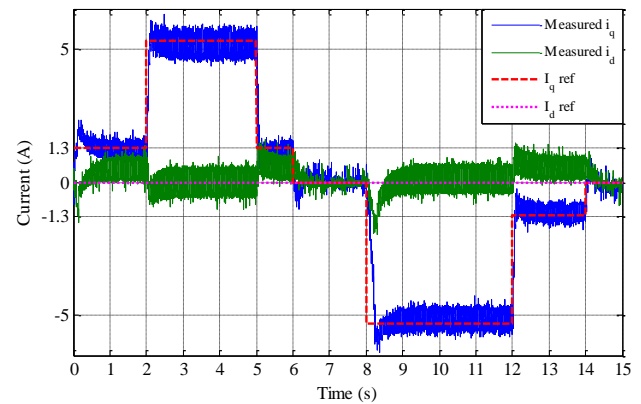


Fig 8b. Measured  $i_q$  and  $i_d$  currents

There is a small d-axis current control error because of the automatic determination of the commutation angle undertaken by the commercial converter, which is about five electrical degrees.

Fig. 9a shows the simulated and EKF estimated  $\theta_e$ , EKF shows a very accurate tracking under load torque. Fig. 9b shows the measured and EKF estimated  $\theta_e$ , the estimated  $\theta_e$  has been used to reconstruct the commutation angle, where the PDD has been successfully operating. The slow harmonic noticed in steady state, which occurs every revolution is caused by eccentricity in the resolver. EKF can provide accurate estimation of the load angle needed to reconstruct the position of the HSR, consequently the PDD could be operated equally well throughout its torque range, without needing to linearize the model around a specific operating point as it is the case for the linear reduced order observer Fig 9c.

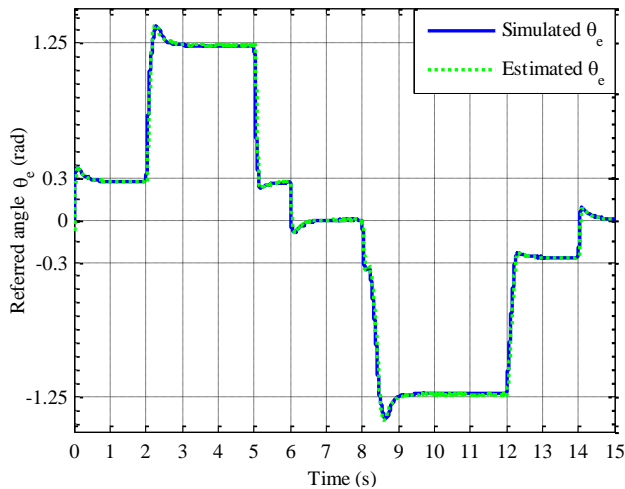


Fig 9a. Simulated and EKF estimated  $\theta_e$

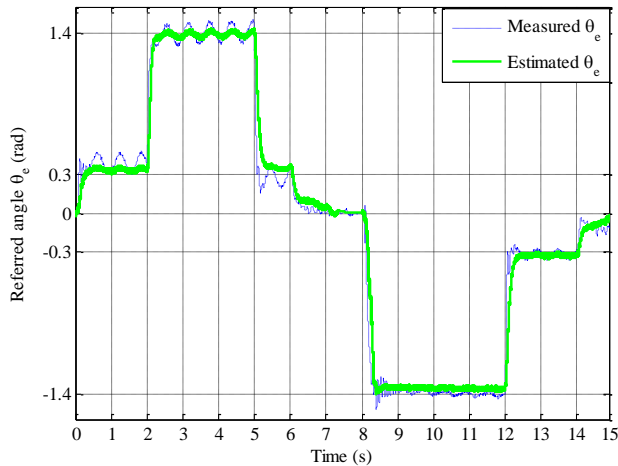


Fig 9b. Measured and estimated  $\theta_e$

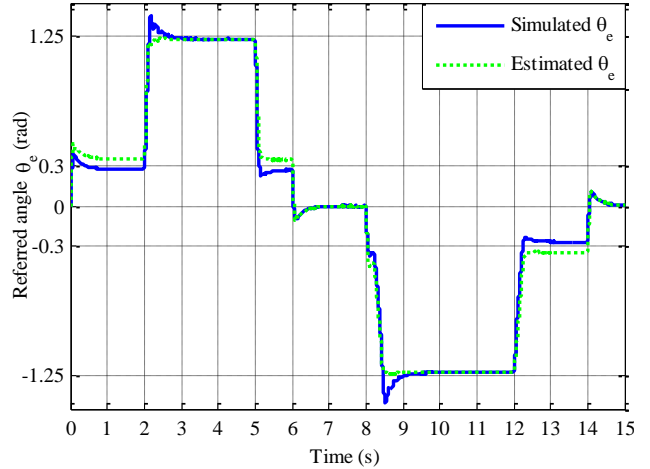


Fig 9c. Simulated and linear observer estimated  $\theta_e$

The experimental results demonstrate that desirable PDD performance has been achieved with the proposed control scheme. It is worth mentioning that the damping effects in the PDD have been neglected in the simulation. This does not result in noticeable differences compared to the measured responses. For the purpose of comparison, Fig. 9c shows the simulated and estimated referred angle  $\theta_e$  obtained with the linear reduced order observer [14]. It is evident that the linear observer can produce good estimation at the linearized operating point around the rated torque but yields noticeable errors when the load torque deviates from the rated value. However, EKF can estimate the referred angle to a larger degree of accuracy for different operating conditions and no significant mismatch is observed. This can improve the accuracy of the estimated HSR position given in (20).

## V. CONCLUSIONS

Extended Kalman Filter has been employed to estimate the states required for full state feedback control of the PDD drive with a position sensor on the LSR. A systematic GA based tuning method for the covariance matrices of the extended Kalman filter has been employed. It has been shown that EKF estimator is capable of tracking the unmeasured states over a wide range of speeds and torques with a high degree of accuracy. This enables the PDD to achieve maximum torque per Ampere operation throughout its operating range. The findings are validated through simulation and experimental results on a prototype PDD.

## VI. REFERENCES

- [1] K. Atallah, J. Rens, S. Mezani, and D. Howe, "A Novel 'Pseudo' Direct-Drive Brushless Permanent Magnet Machine, IEEE Transactions on Magnetics, vol. 44, pp. 4349-4352, 2008.
- [2] D. J. Powell, S. D. Calverley, F. de Wildt, and K. Daffey, "Design and analysis of a Pseudo Direct-Drive

- propulsion motor," in *Power Electronics, Machines and Drives (PEMD 2010)*, 5th IET International Conference on, 2010, pp. 1-2.
- [3] H. Polinder, F. F. A. van der Pijl, G. J. de Vilder, and P. J. Tavner, "Comparison of direct-drive and geared generator concepts for wind turbines," *IEEE Transactions on Energy Conversion*, vol. 21, pp. 725-733, 2006.
- [4] Y. Hori, H. Sawada, and C. Yeonghan, "Slow resonance ratio control for vibration suppression and disturbance rejection in torsional system," *IEEE Transactions on Industrial Electronics*, vol. 46, pp. 162-168, 1999.
- [5] T. M. O'Sullivan, C. M. Bingham, and N. Schofield, "High-Performance Control of Dual-Inertia Servo-Drive Systems Using Low-Cost Integrated SAW Torque Transducers," *IEEE Transactions on Industrial Electronics*, vol. 53, pp. 1226-1237, 2006.
- [6] G. Zhang, "Speed control of two-inertia system by PI/PID control," *IEEE Transactions on Industrial Electronics*, vol. 47, pp. 603-609, 2000.
- [7] T. M. O'Sullivan, C. M. Bingham, and N. Schofield, "Observer-Based Tuning of Two-Inertia Servo-Drive Systems With Integrated SAW Torque Transducers," *IEEE Transactions on Industrial Electronics*, vol. 54, pp. 1080-1091, 2007.
- [8] Y. Jong Nam, S. Jianbo, K. Yong Il, and K. Yong Chun, "Robust Disturbance Observer for Two-Inertia System," *IEEE Transactions on Industrial Electronic*, vol. 60, pp. 2700-2710, 2013.
- [9] L. Harnefors, S. E. Saarakkala, and M. Hinkkanen, "Speed Control of Electrical Drives Using Classical Control Methods," *IEEE Transactions on Industry Applications*, vol. 49, pp. 889-898, 2013.
- [10] S. E. Saarakkala, M. Hinkkanen, and K. Zenger, "Speed control of two-mass mechanical loads in electric drives," in *Energy Conversion Congress and Exposition (ECCE)*, 2012 IEEE, 2012, pp. 1246-1253.
- [11] M. Bouheraoua, J. Wang, and K. Atallah, "Influence of Control Structures and Load Parameters on Performance of a Pseudo Direct Drive," *Machines*, vol. 2, pp. 158-175, 2014.
- [12] R. G. Montague, C. M. Bingham, and K. Atallah, "Characterisation and modelling of magnetic couplings and gears for servo control systems," in *Power Electronics, Machines and Drives (PEMD 2010)*, 5th IET International Conference on, 2010, pp. 1-6.
- [13] R. Montague, C. Bingham, and K. Atallah, "Servo Control of Magnetic Gears," *IEEE/ASME Transactions on Mechatronics*, vol. 17, pp. 269-278, 2012.
- [14] M. Bouheraoua, J. Wang, and K. Atallah, "Speed Control for a Pseudo Direct Drive Permanent-Magnet Machine With One Position Sensor on Low-Speed Rotor," *IEEE Transactions on Industry Applications*, vol. 50, pp. 3825-3833, 2014.
- [15] M. Bouheraoua, J. Wang, and K. Atallah, "A complex frequency domain analysis of a closed loop controlled pseudo direct drive," in *Electrical Machines (ICEM)*, 2012 XXth International Conference on, 2012, pp. 2428-2434.
- [16] W. Leonhard, *Control of Electrical Drives*, 3rd ed.: Springer, 2001.
- [17] M. Bouheraoua, W. Jiabin, and K. Atallah, "Design and implementation of an observer-based state feedback controller for a pseudo direct drive," *IET Electric Power Applications*, vol. 7, pp. 643-653, 2013.
- [18] R. Dhaouadi, N. Mohan, and L. Norum, "Design and implementation of an extended Kalman filter for the state estimation of a permanent magnet synchronous motor," *IEEE Transactions on Power Electronics*, vol. 6, pp. 491-497, 1991.
- [19] J. Jun-Keun and S. Seung-Ki, "Kalman filter and LQ based speed controller for torsional vibration suppression in a 2-mass motor drive system," *IEEE Transactions on Industrial Electronics*, vol. 42, pp. 564-571, 1995.
- [20] S. Bolognani, L. Tubiana, and M. Zigliotto, "Extended Kalman filter tuning in sensorless PMSM drives," *IEEE Transactions on Industry Applications*, vol. 39, pp. 1741-1747, 2003.
- [21] K. Szabat and T. Orłowska-Kowalska, "Application of the extended Kalman filter in advanced control structure of a drive system with elastic joint," in *Industrial Technology, 2008. ICIT 2008. IEEE International Conference on*, 2008, pp. 1-6.
- [22] J. Wang, W. Wang, and K. Atallah, "Kalman filter based sensorless control of a tubular permanent magnet machine for active vehicle suspension," *IET International Conference in Power Electronics, Machines and Drives (PEMD 2010)*, 5th, 2010, pp. 1-6.
- [23] S. Yuchao, S. Kai, H. Lipei, and L. Yongdong, "Online Identification of Permanent Magnet Flux Based on Extended Kalman Filter for IPMSM Drive With Position Sensorless Control," *IEEE Transactions on Industrial Electronics*, vol. 59, pp. 4169-4178, 2012.